

Studies of switching field and thermal energy barrier distributions in a FePt nanoparticle system

X. W. Wu,^{a)} H. Zhou, R. J. M. van de Veerdonk, T. J. Klemmer, C. Liu, N. Shukla, and D. Weller

Seagate Research, 1251 Waterfront Place, Pittsburgh, Pennsylvania 15222-4215

M. Tanase and D. E. Laughlin

Data Storage System Center, Carnegie Mellon University, Pittsburgh, Pennsylvania 15213

(Presented on 13 November 2002)

Dynamic remanent hysteresis loops were measured at several time scales for a $L1_0$ ordered $\text{Fe}_{45}\text{Pt}_{55}$ nanoparticle array sample. At a fixed percentage of magnetization switched, Sharrock's formula was applied to obtain both the thermal stability factor and the intrinsic switching field. From the magnetization dependence of the thermal stability factor, the width of the thermal energy barrier distribution was determined to be about 0.30. In comparison with the particle volume distribution width obtained from transmission electron microscopy, the energy barrier width is reduced significantly due to strong interparticle exchange interaction. The magnetization dependence of the intrinsic switching field was used to obtain the intrinsic, i.e., short time, remanent magnetization curves. The intrinsic switching field distribution width was found to be 0.34. © 2003 American Institute of Physics. [DOI: 10.1063/1.1540041]

I. INTRODUCTION

Recently much attention has been paid to self-assembled and monodisperse FePt nanoparticles for future ultrahigh density magnetic data storage.^{1,2} The chemically ordered FePt $L1_0$ phase is of particular interest because of its high bulk magnetocrystalline anisotropy energy ($K_u \sim 6.6 \times 10^7$ ergs/cm³) that permits smaller particles yet avoids thermal instability.³ As a promising candidate for future magnetic recording media, FePt nanomagnet arrays also have great potential to deliver a much narrower grain size distribution and switching field distribution (SFD), which are crucial factors in achieving a higher signal to noise ratio (SNR). In the literature, noise spectrum techniques have been successfully applied to characterize the SFD in superparamagnetic Co nanoparticle systems.⁴ However, for the $L1_0$ ordered FePt nanoparticle system, this method cannot be applied due to ferromagnetism and sufficient thermal stability. In this article, dynamic remanent hysteresis loops are used to determine both the SFD (determined by the anisotropy energy distribution and the interaction) and the thermal energy barrier distribution (determined by anisotropy energy distribution, grain size distribution, and the interaction) of a chemically ordered $L1_0$ $\text{Fe}_{45}\text{Pt}_{55}$ nanoparticle sample. For a fixed percentage of magnetization switched, Sharrock's formula is used to obtain both the thermal stability factor ($K_u V/k_B T$) and the intrinsic switching field (H_S), from which the thermal energy barrier distribution and the intrinsic switching field distribution can be extracted.

II. $\text{Fe}_{45}\text{Pt}_{55}$ NANOPARTICLE SYSTEM

Chemically disordered as-prepared $\text{Fe}_{45}\text{Pt}_{55}$ nanoparticles were synthesized using the method discussed by Sun

*et al.*¹ It is based on thermal decomposition of iron pentacarbonyl and the reduction of platinum acetylacetonate using a standard airless technique. The particle solution is then washed in ethanol and hexane in the presence of a surfactant oleic acid and oleylamine mixture (1:1) in ambient environment and subsequently deposited onto a silicon substrate with native oxygen. These substrates were used without any prior cleaning or etching. Nanoparticle assemblies are formed after solvent evaporation. The composition of the nanoparticles was determined by the Rutherford backscattering (RBS) technique to be $\text{Fe}_{45}\text{Pt}_{55}$. $L1_0$ chemical ordering is achieved by annealing the sample in a rapid thermal annealing (RTA) furnace at a temperature of 650 °C for 30 min in atmosphere of argon gas with less than 1 ppm of O_2 . The magnetic properties of the sample were studied using superconducting quantum interference device (SQUID) magnetometry. Transmission electron microscopy (TEM) was used to study the microstructures of the annealed particles.

Figure 1 exhibits the hysteresis (solid line) and remanent hysteresis (dashed line) loops measured at room temperature with the field applied parallel to the substrate. It shows coercivity H_C of 3 kOe and remanent coercivity H_{CR} , defined as the reverse field applied where $M_r=0$, of 5 kOe. The measured squareness S of the sample is about 0.62. The $L1_0$ chemical ordering is confirmed by x-ray diffraction. The relatively low H_C for the ordered $\text{Fe}_{45}\text{Pt}_{55}$ nanoparticles is due to the off-stoichiometry composition. We have also measured both magnetic hysteresis loops along the perpendicular direction (not shown here), and they show identical behavior to the curves along the parallel direction. This suggests that the annealed particles possess three-dimensional (3D) random magnetic anisotropy. The same 3D random anisotropy has also been confirmed by x-ray diffraction measurements. For a noninteracting 3D random system, the squareness of

^{a)}Electronic mail: xiaowei.wu@seagate.com

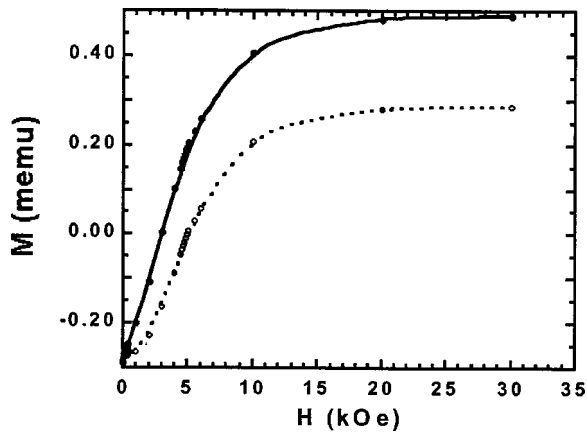


FIG. 1. Hysteresis (solid line) and remanent hysteresis (dashed line) loops of an annealed $\text{Fe}_{45}\text{Pt}_{55}$ sample measured with magnetic field applied in the plane of the substrate.

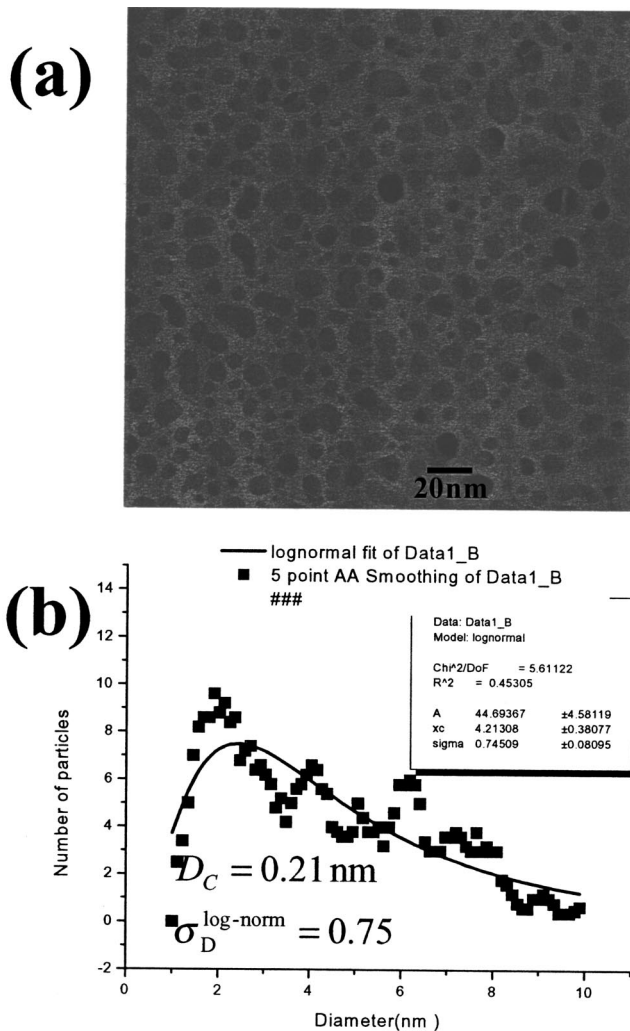


FIG. 2. (a) TEM image of the $\text{Fe}_{45}\text{Pt}_{55}$ nanoparticle system. (b) Log-normal distribution of the $\text{Fe}_{45}\text{Pt}_{55}$ nanoparticles obtained from the TEM image. It shows a mean diameter of 4.2 nm and a size distribution width of 0.75.

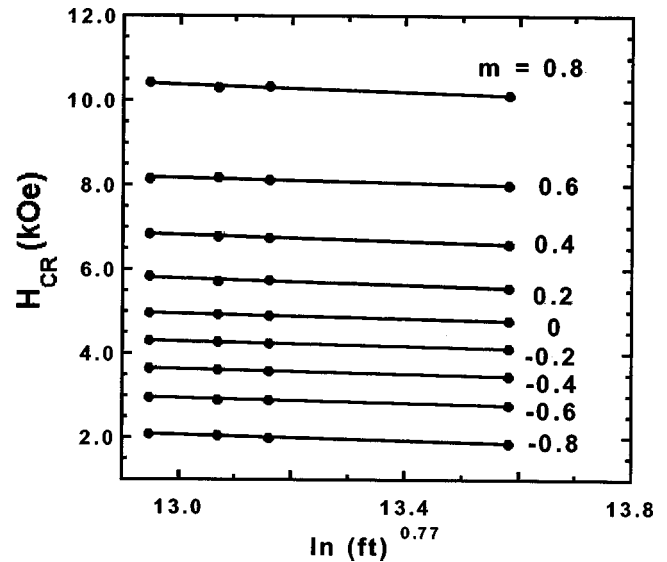


FIG. 3. Time dependence of the applied field for different magnetization levels. The solid lines are linear fits to the data.

the hysteresis loop should be close to 0.5. The higher squareness ($S=0.62$) in this $\text{Fe}_{45}\text{Pt}_{55}$ nanoparticle system indicates the existence of strong interparticle exchange interactions.⁵ Figure 2(a) shows a TEM image of the $\text{Fe}_{45}\text{Pt}_{55}$ particles annealed under the same conditions on a TEM grid. The image shows severe particle sintering, which occurs during the annealing process.⁶ Both the self-assembly and monodisperse properties of the $\text{Fe}_{45}\text{Pt}_{55}$ nanoparticles deteriorated due to this sintering process. The sintering process is also responsible for strong interparticle exchange interactions. Assuming a log-normal particle size distribution, from the TEM image, the mean diameter of the particles is about 4.2 nm and the size distribution width ($\sigma_{\text{size}}^{\text{log-normal}}/\langle \text{size} \rangle$) is estimated to be 0.75 [shown in Fig. 2(b)]. Assuming the sintering process and the size distribution of the silicon wafer are similar to those on the TEM grid, the volume distribution of the sample used for the magnetometer would be close to $\sigma_V^{\text{log-normal}}/\langle V \rangle = 3 \times \sigma_{\text{size}}^{\text{log-normal}}/\langle \text{size} \rangle = 2.20$.

III. MEASUREMENT RESULTS AND DISCUSSIONS

Dynamic remanent hysteresis loop measurements have been applied to obtain the thermal energy barrier distribution in both longitudinal and perpendicular media.⁷⁻⁹ In general, a saturation field is first applied to put the sample in the saturated remanent state. A reverse field H_r is then applied for a fixed time duration t , and finally the remanent magnetization M_r is recorded after removal of the external field. Due to thermal relaxation of the system, with an increase in the duration of the field applied, the remanent coercivity decreases. For a fixed magnetization level, the thermal stability factor $K_u V/k_B T$ can be obtained from Sharrock's formula for 3D randomly oriented media:¹⁰

$$H(m, t) = H_S(m) \left[1 - \left(\frac{k_B T}{K_u V_{\text{eff}}(m)} \ln(f_0 t) \right)^{0.77} \right]. \quad (1)$$

Here, due to the high anisotropy energy of the $L1_0$ structure, an attempt frequency of $f_0 = 10^{10} \text{ s}^{-1}$ is assumed for FePt

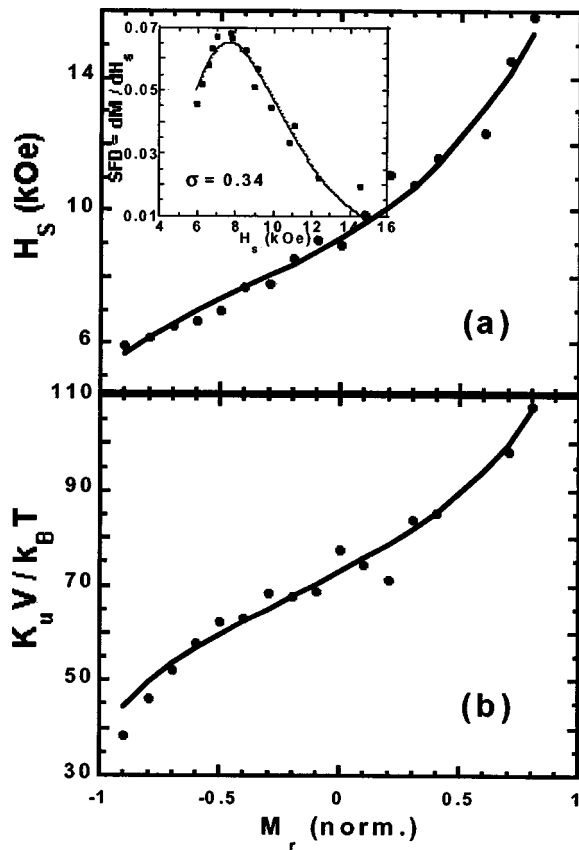


FIG. 4. (a) Intrinsic coercivity H_S vs the magnetization level for $\text{Fe}_{45}\text{Pt}_{55}$. The points measured are shown as closed circles. The inset shows dm/dH_S vs H_S , indicating the intrinsic SFD of the sample. The solid line is a log-normal fit with $\beta_{\text{SFD}}=0.34$. (b) Thermal stability factor $K_u V/k_B T$ vs the percentage of magnetization switched for $\text{Fe}_{45}\text{Pt}_{55}$. The solid line is the using $\beta_{KV}=0.30$.

nanoparticles, which is one order of magnitude higher than that typically used in current recording media.⁹ $H_S(m)$ is the intrinsic switching field at a fixed normalized magnetization level $m = M_r/M_{r,\text{sat}}$. The time range for the dynamics remanent hysteresis loop measurements is intrinsically limited by the characteristic time (about 120 s) of the SQUID magnetometer. The wait times employed in the present experiment are between 120 to 720 s.

In Fig. 3, the reverse field applied is plotted versus $\ln(f_0 t)^{0.77}$ from 10% ($m=0.8$) to 90% ($m=-0.8$) of magnetization switched. The linearity of all curves (shown as the solid lines in Fig. 3) indicates that Sharrock's formula, Eq. (1), is a good approximation.

By fitting each curve in Fig. 3 using Eq. (1), we can obtain the magnetization dependence of both $H_S(m)$ and the thermal stability factor $K_u V_{\text{eff}}(m)/k_B T$, as shown in Figs. 4(a) and 4(b), respectively. The intrinsic switching field H_S increases from 6 kOe at 10% switching ($m=-0.8$) to 16 kOe at 90% switching ($m=0.8$) with $H_S=9$ kOe at 50% switching ($m=0$). The thermal stability factor increases from 45 at 10% switching ($m=-0.8$) to about 110 at 90% switching ($m=0.8$) with $K_u V_{50}/k_B T=70$ at 50% switching ($m=0$). The magnetization dependence of H_S provides information

about the intrinsic SFD (without any thermal effect). The inset in Fig. 4(a) is the $\text{SFD}=dm/dH_S$ obtained from the magnetization dependence of H_S . It follows a log-normal distribution quite well, and has a distribution width $\sigma_{\text{SFD}}/\langle\text{SFD}\rangle$ of about 0.34 (indicated by the solid line).

For a weakly coupled system, the energy barrier distribution $\rho(E)$, where $E=K_u V_{\text{eff}}$, should also exhibit a log-normal distribution with constant width $\sigma_{KV}^{\text{log-normal}}/\langle KV \rangle$, which reflects the effect of the physical particle size distribution, K_u distribution, as well as the interparticle interactions.^{9,11} The solid line in Fig. 4(b) is the curve fitted using a log-normal distribution for the energy barrier using $\sigma_{KV}^{\text{log-normal}}/\langle KV \rangle=0.3$. In comparison with the particle volume distribution ($\sigma_V^{\text{log-normal}}/\langle V \rangle \sim 2.20$), the thermal energy barrier distribution width has been greatly reduced. This dramatic reduction of the energy barrier width is likely due to intergranular exchange coupling, which has also been observed in perpendicular media.^{9,11} We also would like to point out that, compared to what we observed in perpendicular media, the reduction in the $\text{Fe}_{45}\text{Pt}_{55}$ system is much greater. This could be an indication of a possible incoherent switching process within each sintered particle.

IV. CONCLUSION

Magnetic properties and microstructures of a $\text{Fe}_{45}\text{Pt}_{55}$ nanoparticle system were studied. The sample exhibits 3D random magnetic anisotropy. Strong sintering and interparticle exchange interactions are evident after the annealing process. Dynamic remanent hysteresis loops at different applied field strengths and durations were used to determine both the SFD and the thermal energy barrier distribution. Sharrock's formula for 3D random anisotropy is found to be applicable to all levels of magnetization switched. The SFD width was estimated to be 0.34. The thermal energy barrier distribution width was about 0.30. In comparison with the particle area distribution width obtained from the TEM image, the energy barrier distribution width is greatly reduced due to strong interparticle exchange interaction.

- ¹S. Sun, C. B. Murray, D. Weller, L. Folks, and A. Moser, *Science* **287**, 1989 (2000).
- ²S. Sun, D. Weller, and C. Murray, in *The Physics of Ultra-High-Density Magnetic Recording*, edited by M. L. Plumer, J. van Ek, and D. Weller (Springer, New York, 2001), pp. 249–276.
- ³D. Weller and A. Mose, *IEEE Trans. Magn.* **35**, 4423 (1999).
- ⁴S. I. Woods, J. R. Kirtley, S. Sun, and R. H. Koch, *Phys. Rev. Lett.* **87**, 137205 (2001).
- ⁵R. W. Chantrell, D. Weller, T. J. Klemmer, S. Sun, and E. F. Fullerton, *J. Appl. Phys.* **91**, 6866 (2002).
- ⁶T. J. Klemmer, N. Shukla, C. Liu, X. W. Wu, E. B. Svedberg, O. Mryasov, R. Chantrell, and D. Weller, *Appl. Phys. Lett.* (to be published).
- ⁷B. E. Higgins, A. F. Torabi, and M. L. Mallery, *IEEE Trans. Magn.* **37**, 1528 (2001).
- ⁸H. J. Richter, R. M. Brockie, and J. L. Pressesky, *IEEE Trans. Magn.* **38**, 260 (2002).
- ⁹X. W. Wu, H. Zhou, R. J. M. van de Veerdonk, G. Ju, B. Lu, and D. Weller, *Appl. Phys. Lett.* **81**, 2409 (2002).
- ¹⁰M. P. Sharrock, *J. Appl. Phys.* **76**, 6413 (1994); H. Pfeiffer, *Phys. Status Solidi A* **118**, 295 (1990).
- ¹¹H. Zhou, H. N. Bertram, and M. E. Schabes, *J. Appl. Phys.* **91**, 8378 (2002).